



Dimethyl sulfide (DMS) climatologies, fluxes and trends - Part A: Differences between seawater DMS estimations

Sankirna D. Joge^{1,2}, Anoop S. Mahajan^{1,*}, Shrivardhan Hulswar¹, Christa A. Marandino³, Martí Galí^{4,5}, Thomas G. Bell⁶ and Rafel Simo⁴

5 ¹Indian Institute of Tropical Meteorology, Pune, India

²Savitribai Phule Pune University, Pune, India

³Research Division 2-Biogeochemistry, GEOMAR Helmholtz Centre for Ocean Research Kiel, Kiel, Germany

⁴Institut de Ciències del Mar (CSIC), Barcelona, Catalonia, Spain

⁵ Barcelona Supercomputing Center (BSC), Barcelona, Spain

10 ⁶Plymouth Marine Laboratory (PML), Plymouth, UK

*Correspondence to: Anoop S. Mahajan (anoop@tropmet.res.in)

Abstract: Dimethyl sulfide (DMS) is a naturally emitted trace gas that can affect the Earth's radiative budget by changing cloud albedo. Most models depend on regional or global distributions of seawater DMS concentrations and sea-air flux parameterizations to estimate its emissions. In this study, we analyze the differences between three estimations of seawater DMS, one of which is an observation-based interpolation method (Hulswar et al., 2022 (hereafter referred to as H22)) and two are proxy-based parameterization methods (Galí et al., 2018a (G18); Wang et al., 2020 (W20)). The interpolation-based method depends on the distribution of observations and the methods used to fill data between observations, while the parameterization-based methods rely on establishing a relationship between DMS and environmental parameters such as chlorophyll a, mixed layer depth, nutrients, sea surface temperature, etc., which can then be used to predict DMS concentrations. On average, the interpolation-based methods show higher DMS values compared to the parameterization-based methods. Even though the interpolation method shows higher values than the parameterization-based methods, it fails to capture mesoscale variability. The regression-based parameterization method (G18) shows the lowest values compared to other estimations, especially in the Southern Ocean, which is the high DMS region in Austral summer. The parameterization-based methods suggest significant positive long-term trends in seawater DMS ($6.94 \pm 1.44\%$ decade⁻¹ for G18 and $3.53 \pm 0.53\%$ decade⁻¹ for W20). Since large differences, often more than 100%, are observed between the different estimations of seawater DMS, the derived sea-air fluxes and hence the impact of DMS on the radiative budget are very sensitive to the estimate used.



1 Introduction

30 Seawater dimethyl sulfide (DMS) is a major source of sulfate aerosols in the marine atmosphere (Bates and Quinn, 1997). It is a by-product of the phytoplankton life cycle and marine microbial food web interactions (Andreae and Crutzen, 1997; Simó, 2001). A significant part of the produced DMS is either oxidized by photochemical reactions or metabolized by bacteria (Toole et al., 2003), and the rest is released into the atmosphere as gaseous DMS (Galí and Simó, 2015; Simó, 2001). In the atmosphere, DMS oxidizes to form sulfuric and methane sulfonic acid, eventually leading to aerosol formation and growth. These aerosols can act as cloud condensation nuclei (CCN), especially in environments remote from anthropogenic and continental influence (Andreae and Barnard, 1984; Korhonen et al., 2008). Thus, DMS ultimately affects the incoming solar radiation by increasing/decreasing cloud albedo over the oceans and due to this DMS concentrations in seawater decrease/increase (Vallina and Simó, 2007). This feedback cycle is referred to as the CLAW hypothesis (Charlson et al., 1987; Wang et al., 2018b).

40 The emission of DMS into the atmosphere is an important sea-air interaction process and determines the impact of seawater DMS on the global radiation budget (Stefels et al., 2007; Saint-Macary et al., 2022). In most global models, this flux is estimated as a product of the seawater DMS concentration and a parameterization of the sea-air flux transfer velocity (Liss, 1983; Johnson, 2010). Considering that seawater DMS concentration is an essential part of the flux calculation, its accurate estimation plays a crucial role in quantifying the impact of DMS on cloud formation. Regional and global distributions of seawater DMS concentrations are estimated using observation-based interpolation, process-level modeling, and parameterization-based approaches (Belviso et al., 2004b).

45 In the interpolation-based approach, the global seawater DMS distribution is estimated by interpolating/extrapolating all available in situ DMS observations. The first observation-based climatology was published by Kettle et al. (1999) and used only about 15,000 observations globally. Observations were segregated using static biogeochemical province boundaries defined by Longhurst et al. (1995) and then interpolated across province boundaries and individual grid points. A similar approach was followed by Lana et al. (2011), although the number of data points used in this study had increased by 3-fold (47,000 observations). Hulswar et al. (2022) recently presented an updated version, i.e., the third climatology, using an interpolation-based approach. This recent climatology was created with an ~18-fold increase in observations (870,000 observations) and included significant updates in the filtering and data unification process. They also included dynamically changing seasonal biogeochemical province boundaries (Reygondeau et al., 2013) to capture spatial/temporal changes in biogeochemistry, especially along the borders of provinces. The interpolation lengths for this climatology are based on observed DMS variability length scales (VLS) (Royer et al., 2015; Manville et al., 2023), which produce more realistic geographical distributions.

55 In process-level models, the estimation of DMS is done using mathematical relationships at small scales between many biogeochemical and environmental parameters to define how DMS production and destruction occurs. This method is complex due to the non-linear relationship between DMS, proxy-parameters, and its main precursor, dimethylsulfoniopropionate

60

(DMSP). The biogeochemical cycle of nutrients and the spatiotemporal distribution of different plankton taxa plays an important role, and these are modelled across the globe using a detailed biogeochemical model, which predicts the seawater DMS concentrations (Anderson et al., 2001; Belviso et al., 2004b; Wang et al., 2018a). These estimations are inherently linked to our understanding of the underlying processes controlling DMS production and loss and hence, can be highly biased if these processes are not well described in the model (Galí et al., 2023). This method is also computationally expensive. The models based on this approach lead to DMS climatologies of resolutions, which are dependent on their parent model but are usually to the order of $0.25^{\circ} \times 0.25^{\circ}$ and hence can include mesoscale dynamic changes.

Finally, in the parameterization-based approach, a parametric equation between DMS/DMSP and single or multiple variables (biogeochemical/environmental parameters) is defined through linear/multi-linear regression at a larger scale. This approach is simple to implement compared to process-level models and can work more efficiently than observation-based interpolation for capturing mesoscale changes and understanding trends (Belviso et al., 2004a). Initial attempts were made in the early 2000s, with Simó and Dachs (2002) using chlorophyll-a and mixed layer depth (MLD) as proxies for predicting DMS. Later, Vallina and Simó (2007) additionally used surface irradiance as a predictor due to a strong relationship observed between DMS and the solar radiation dose over the global surface ocean. A recent study focused on the relationship between DMSP and satellite-based data of chlorophyll-a, SST, particulate inorganic carbon (PIC), and MLD. Different parameterizations in both stratified and mixed water columns were established through regression analysis (Galí et al., 2015). Later, DMS values were estimated across the oceanic biomes as a function of estimated DMSP and the satellite-based data of photosynthetically available radiation (PAR) using a similar regression analysis (Galí et al., 2018). An upgrade to this method is using machine learning, such as an artificial neural network (ANN) (Wang et al., 2020b) or Gaussian process regression (GPR) (Mansour et al., 2023) to create the parameterization. The climatology in these cases is created by training the machine learning algorithms in data-rich regions. While ANN is more expensive in computation than regression analysis, it is less expensive than process-level models. The parameterization approach used within modelling simulations (Halloran et al., 2010) shows that the method is not applicable in all conditions for estimating DMS. The biggest disadvantage of the ANN method is that it requires a large number of observations to train the model efficiently; also, it fails to explain the processes behind the interconnected input, hidden and output layers. A series of sensitivity tests between DMS and the individual parameters need to be run to check whether a change in a single parameter gives a unidirectional response for the predicted DMS values (Wang et al., 2020b). We selected the latest interpolation-based (Hulswar et al., 2022) and two parameterization-based DMS estimations (Galí et al., 2018; Wang et al., 2020b) to study the relative differences in the absolute values of the estimations, their geographical differences and compare the long-term trends.



2 Methods

In this study, we compare three seawater DMS estimations created using two methods: i.e., an interpolation-based Hulswar et al. (2022) climatology, hereafter referred to as H22 (<https://doi.org/10.17632/hyn62spny2.1>) and two parameterization-based estimates, Galí et al. (2018) climatology, hereafter referred to as G18 (<https://doi.org/10.5281/zenodo.2558511>), and Wang et al. (2020a) climatology, hereafter referred to as W20 (<https://doi.org/10.5281/zenodo.3833233>) (Wang et al., 2020a).

For G18 and W20, the monthly estimations are obtained using a parameterized relationship between DMS and different environmental parameters. These parameters include sea surface temperature (SST), salinity, and nutrients such as phosphate, nitrate, and silicate from WOA 2018 (<https://www.ncei.noaa.gov/access/world-ocean-atlas-2018/>) at a $1^\circ \times 1^\circ$ monthly resolution, MLD from MIMOC (<https://www.pmel.noaa.gov/mimoc/>; $0.5^\circ \times 0.5^\circ$ and monthly resolution), and satellite-based variables from NASA SeaWiFS (<https://oceancolor.gsfc.nasa.gov/13/>; 9×9 km and monthly resolution) for chlorophyll a, PAR, euphotic depth, and PIC. The DMS climatologies for W20 and G18 were created at a one-degree resolution, similar to H22. Hence the input data was also interpolated to one degree. The calculations for G18 and W20 were done to get monthly estimates from 1998 to 2010 in order to estimate the long-term trends in seawater DMS. In the case of G18, the $DMSP_t$ values were calculated based on the equations given by Galí et al. (2015), and then DMS monthly values were calculated using globally optimized coefficients for the parametric equation for $DMSP_t$ to DMS conversion (Galí et al., 2018). For W20, we used the best combination that was determined by Wang et al. (2020) to train the model, resulting in an $R^2 = 0.66$. The monthly climatologies were then computed for G18 and W20, which enabled direct comparison with H22.

The decadal trend for G18 and W20 is calculated using the bootstrap resampling method (Geiger et al., 2002). Before applying the bootstrap method, the seasonal variation is removed from the DMS time-series dataset. For this, the mean values of each month are calculated for the period 1998-2010 and then subtracted from the corresponding month of each year. This results in anomalies used for calculating the trend using the bootstrap resampling method. The bootstrap method randomly selects samples ($n=100$) with replacement from the entire anomaly data which is present from 1998 to 2010. These samples are fitted over a first-order polynomial, and the corresponding gradient (trend) and intercept are obtained for each sample set. After this, mean trend (B) and corresponding standard deviation (σ_B), as well as the mean intercept and its corresponding standard deviation are calculated. The t_b value is obtained by taking the ratio of the mean trend (B) and its corresponding standard deviation (σ_B), i.e. $t_b = |B/\sigma_B|$. If the t_b value is greater than 2 then the significance level of trend and its intercept are considered to be better than 95 % (Weatherhead et al., 1998). This method has been used to calculate long-term trends in the past (Mahajan et al., 2015).

3 Results and discussions

3.1 Differences between the DMS climatologies



The seasonal and geographical variation in the three seawater DMS climatologies is shown in Figure 1a. Broadly, the seasonal variation is dominated by the available solar radiation, with peaks in the northern hemisphere during June-July-August (JJA) and peaks in the southern hemisphere during December-January-February (DJF). The maximum DMS values observed in the polar regions during their respective summers have been attributed to the melting of ice that releases nutrients at the time of maximal light availability (Hawkings et al., 2020; Becagli et al., 2016; Zhang et al., 2021; Park et al., 2019; Gourdal et al., 2018; Sørensen et al., 2017), which causes phytoplankton blooms in the Arctic and Antarctic coastal regions. Figure 1b shows the histogram of DMS concentrations. For all the climatologies, most pixels show DMS concentrations < 3 nM in the oligotrophic regions and higher concentrations along the coastal regions and regions with higher nutrient availability.

During the austral summer season (DJF), H22 shows a uniform increase in the Antarctic circle and the Southern Ocean. By comparison, G18 does not show a peak in coastal Antarctica or the Southern Ocean probably because of $1^{\circ} \times 1^{\circ}$ re-gridding and this underestimation has been discussed in detail in Galí et al. (2018). Instead, a band of elevated DMS is seen in the South Atlantic and Indian Oceans centered around the 45° S latitude as the satellite data of chlorophyll may be biased towards colored dissolved organic matter (CDOM) and detritus on the Argentinian basin. (Astoreca et al., 2009; Hayashida et al., 2020; Bock et al., 2021). This region is the transition between subtropical and subpolar waters and is also known for hosting high abundances of DMS produces like coccolithophores and also the important role of dinoflagellates into this region (Balch et al., 2016). W20 shows a distribution similar to H22, albeit with lower DMS values in most regions and higher values in the Ross Sea and Weddell Sea regions compared to the Indian sector of the Southern Ocean. The histogram distribution (Fig. 1b) also shows that H22 predicts higher values than the other two climatologies, with the highest number of pixels in the 3-4 nM range and more than 2000 pixels showing concentrations above 6 nM, while G18 has less than 300 pixels with concentrations above 6 nM (Fig. 1b). For G18, the pixels with higher concentrations are in the southern mid-latitude region or coastal regions (Fig. 1a), while for the other climatologies, most of these values are in the Southern Ocean and coastal Antarctica. G18 and W20 show fewer pixels with concentrations larger than 6 nM as compared to H22 (Fig. 1b).

A similar variation can be observed during the boreal summer season (JJA) in the northern hemisphere, where high concentrations of DMS are present in the Arctic circle in all climatologies (Fig. 1a). The geographical distribution in the northern hemisphere during summer is similar for H22 and W20, with peaks observed east of Greenland, off the coast of Alaska, and high values in the Arctic (Park et al., 2018). W20 shows peak values along the Northern coastal regions of Russia in Kara sea, Laptev sea region compared to H22. G18 shows peak values in Corne sea, Celtic sea region. Both G18 and W20 show high local peaks of DMS concentration compared to H22. In terms of histogram distribution, G18 shows approximately 600 pixels with DMS concentration less than 6 nM while W20 shows up to 800 pixels. For H22, this pixel count is approximately 800. It can also be observed that G18 and W20 also captured DMS values more than 8 nM while in H22 there were no values that high. (Fig. 1b). The peak values observed during the boreal summer are lower than during the austral summer, with fewer pixels showing values above 6 nM for all the climatologies.

During boreal spring (March-April-May (MAM)) and autumn (September-October-November(SON)), there is a gradual increase in DMS concentrations in the northern and southern hemispheres, as seen in Figure 1a. The number of pixels with



155 concentrations larger than 6 nM is low for all the climatologies (Fig. 1b). The H22 climatology shows higher values along the coastal upwelling regions, such as South America's west coast and Africa's southwest coast (Fig. 1a), which was observed in previous studies. For example, the DMS concentration in the waters of Peru upwelling region (Andreae, 1985; Riseman and DiTullio, 2004), the highest DMS concentration in coastal upwelling areas of the west coast of India (Shenoy and Kumar, 2007), North Africa, Angola, Peru and Equatorial Pacific Ocean is also observed (Kettle et al., 1999), Mauritanian upwelling is a hotspot for DMSP and thus DMS which underlines coastal upwelling region as a local source for seawater DMS (Zindler et al., 2012). During SON, a peak is also seen in the Indian Ocean by all the climatologies due to the physical forcing generated by monsoon wind in the form of upwelling, which results in high biological production (Shenoy et al., 2002; Shenoy and Kumar, 2007), although G18 shows higher values in the Atlantic and Pacific too, which is missing in the other estimations. The area weighted global DMS mean for the climatologies are 2.28 nM for H22, 1.69 nM for G18, and 1.75 nM for W20.

160 Thus, the two parameterization-based estimations show significantly lower global weighted mean concentrations than the interpolation-based estimations. However, the parameterization-based estimations show higher peak values; for example, the maximum value during DJF is 18.67 nM in the Weddell Sea for H22 but is higher at 18.94 nM off the coast of Chile in South Pacific ocean for G18 and 23.64 nM in the Gulf of Mexico for W20. The maximum DMS during JJA for H22 is 7.29 nM in the Norwegian Sea, while for G18, the peak is 15.84 nM in the Chorne sea and 46.23 nM in the Kara Sea for W20. This shows that although globally averaged concentrations are higher in the interpolation-based method, the concentrations over individual pixels can be much larger for the parameterization-based approach. The main reason for this is the bin-based averaging of observations done in the interpolation-based approach to remove very localized high values that would have a disproportionate weight on regional and global averages. Due to this, no pixels higher than 8 nM are observed in H22 in MAM, JJA and SON (Fig. 1b). Also, a sampling bias is inherent to the interpolation-based method, as discussed by Galí et al. (2018). Thus, the parameterization-based approach has an advantage, where they can capture large point emissions during periods of high productivity. These high point emissions are likely to affect local and regional new particle formation on shorter timescales. Figure 2a shows the difference between H22 and the other two climatologies. In the Southern Ocean, H22 predicts a higher value of DMS concentration with larger positive differences with G18 and W20. In DJF, large negative differences can also be observed with G18 in Argentinian Shelf region and coastal areas of Peru and Chile. Similarly, positive differences can also be seen in the JJA season, with some negative differences in the case of W20 in the Arctic Circle and negative differences with G18 along some coastal areas of continents. The histogram of differences is centered around zero, showing that most pixels show a minor change, although large differences of > 10 nM are also seen in some pixels, especially during DJF. The differences between H22 and G18 or W20 (Fig. 2b) are not centered around zero, with most pixels showing higher values in the H22 estimation. Some pixels show a negative difference in the Arctic Ocean, south Atlantic, and South Australian basin mostly along high-productivity coastal regions. From all the seasons, the maximum difference between H22 and G18 is -14.74 nM during DJF in the Argentinian basin region and -29.03 nM for W20 during MAM in the Arctic Sea. Overall, G18 and W20 show a significantly lower estimation than H22 in Antarctic coastal area, but G18 shows significantly higher values in coastal

165
170
175
180
185



regions of other continents such as in South America in the coastal areas of Peru and Chile, Argentina basin and northern coastal regions of Russia.

190 3.2 Latitudinal Variations

The latitudinal variations of globally averaged seawater DMS climatologies for each month are shown in Figure 3. We checked the variations according to six latitudinal regions, i.e., northern polar region ($> 60^\circ$ N) and southern polar region ($< 60^\circ$ S), northern mid-latitude region (30° N to 60° N) and southern mid-latitude region (30° S to 60° S), northern equatorial region (0° to 30° N) and southern equatorial region (0° to 30° S). All the climatologies show a similar annual trend in all the regions, although considerable differences are observed in the polar regions.

195 In the northern polar region, H22 surprisingly shows a lower mean DMS value (1.73 nM) in April compared to February and May (Fig. 3a). This is most likely due to faulty interpolation in H22, which indicates that observation-based interpolation methods can become biased if incorrect mapping is done. In the same region, a maximum mean value of 4.20 nM is observed in June, which is closer to G18 (4.04 nM) but higher than H22 (3.41 nM). H22 estimates high mean values in January, February, 200 March, November and December compared to G18 and W20. The W20 estimations closely match the interpolation-based estimations in the boreal summer months although both G18 and W20 follow the same pattern, lower values are observed in the winter months of DJF compared to H22. Considering the low sunlight during this period, the means suggest that the interpolation-based methods overestimate the DMS concentrations during winter, while W20 estimations seem more likely. This bias is most likely due to interpolation rather than a sampling bias.

205 Large differences are observed in the Southern Ocean between the interpolation-based and parameterization-based climatologies. With much increased data availability in the Southern Ocean owing to the high-frequency observations obtained using membrane inlet mass spectroscopy (MIMS), the updated DMS climatology in Jarníková and Tortell (2016), which was created using new high-frequency observation data in the Southern Ocean shows higher concentration in high latitudinal regions. The differences may reach over +10 nM in some regions, like the Weddell Sea and the waters around the Balleny 210 Islands, while large decreases by over -10 nM may appear in other regions of the Ross and the Bellingshausen Seas. Although all the climatologies show higher values during the austral summer months, H22 (peak: 12.3 nM in January) shows significantly higher values as compared to G18 (peak: 1.81 nM in December) and W20 (peak: 4.69 nM in December). G18 struggles to simulate accurate concentrations, suggesting that this method fails in southern polar regions (Fig. 3b). W20 shows an increase, although this is driven by higher concentrations in particular regions, such as the Ross Sea, as compared to more generalized larger concentrations along the entire Antarctic coastline, as seen in H22 (Fig. 1a).

215 For the northern mid-latitude region, H22 shows values peaking at 4.57 nM (in May). W20 also shows an increase in the summer with values in the range of 2.75 nM (in May) to 3.73 nM (in August). G18 shows values ranging from 2.61 nM (in August) to 3.76 nM (in May) and peaking at 4.11 nM in June (Fig. 3c). In the southern mid-latitude region, which covers the southern Pacific, Atlantic, and Indian Oceans, H22 estimates a range from 2.96 nM in November to 3.88 nM in January. 220 Estimates for G18 and W20 are similar, with peaks appearing in the austral summer months (between ~2-3 nM; Fig. 3d).



Although the means are similar for these two estimates, the geographical distribution is different, with G18 shows a band of increased DMS along the 45°S latitude while W20 shows increases along Africa and the Pacific.

The equatorial regions show the lowest mean concentrations of all the latitudinal regions. In the northern equatorial region, all the climatologies show a similar estimation with values ranging between 1-2.5 nM. G18 shows lower values, especially from August to December. For the southern equatorial region, H22 peaks at 3.04 nM in December while W20 and G18 show lower values, although, similarly to other regions, G18 gives the lowest values of the three from February to July for these latitudes' region.

3.3 Long-term trend

The long-term trends in DMS for G18 and W20 are shown in Figure 4. High-resolution data is important for time series analysis to observe variations. We used monthly chlorophyll a, PAR, and PIC data along with climatological data of nutrients, MLD, and SST on which G18 and W20 are developed in order to compare the trends. For G18 and W20, the trend is calculated after removing the seasonal signal from the time series for data between 1998 and 2010. G18 (Fig. 4a) and W20 (Fig. 4b) show significant increasing trends of 6.94 ± 1.44 % decade⁻¹ ($t_b = 4.82$) and 3.53 ± 0.53 % decade⁻¹ ($t_b = 6.71$), respectively. This suggests an increase in globally averaged seawater DMS concentrations across the world's oceans. In the case of G18, the calculations are done using the globally optimized coefficients (Galí et al., 2018). If the same calculations are done using coefficients optimized for > 45° N (Fig. S1), then the calculated trend is 7.20 ± 1.90 % decade⁻¹ ($t_b = 3.80$). Thus, the trend in the W20 climatology is nearly 50 % lower than the trend observed by G18, probably due to the differences in the parameterization scheme and its sensitivity of coefficient values for the different predictors in both methods. It should be noted that the radiative forcing of past and future DMS driven aerosol formation is uncertain. The IPCC AR5 concluded that a negative feedback of -0.02 W m⁻² °C⁻¹ is expected (IPCC, 2014), with DMS emissions expected to increase with global warming. The AR6, in contrast, suggests that DMS emissions are expected to decrease, resulting in a positive feedback of 0.005 [0.0 to 0.01] W m⁻² °C⁻¹ (IPCC, 2021) due to a decrease in ocean productivity. The results presented here show an increasing trend in the seawater DMS concentrations from 1998 to 2010 and suggest that more research is needed to understand the drivers of seawater DMS before an accurate estimation of its impacts in the future can be made. SeaWiFS satellite data is available only from 1998 to 2010 and same limitation is with other satellite products which starts from 2002 onwards. Hence, there is limitation for the past and future projection of DMS values due to availability of satellite-based predictors for limited years. This issue can be resolved with the predictors obtained from CMIP5 and CMPI6 reconstructed models so that projections can be obtained from past (1850 CE) to future (2100 CE).

3.4 Comparison with other climatologies

Over the last two decades, diagnostic or prognostic models, or models that are prognostic but use empirical modules to predict DMS, have been used to quantify the impact of DMS (Collins et al., 2011; Kloster et al., 2006; Six and Maier-Reimer, 2006; Vogt et al., 2010; Elliott, 2009). Hence, to compare the results from the observation-based interpolation method (H22),



regression-based parametrization (G18), and machine learning based parametrization (W20), we choose only models that are either prognostic or diagnostic.

255 Aumont et al. (2002) were the first to apply a process model parametrization for global DMS using chlorophyll and community structure index derived from a global biogeochemical model with a variable horizontal grid from 0.5° to 2°. This method estimated a weighted annual mean DMS of 1.70 nM. Chu et al. (Chu et al., 2003) simulated the production and destruction of DMS by producing DMSP_d through planktonic excretion of DMSP, which yields DMS through lysis. The DMS sinks included photolysis, bacterial consumption, and gas exchange at the air-sea interface, giving a high resolution (0.28°×0.28°) estimate of
260 DMS across the world's oceans. This prognostic model resulted in a weighted annual global mean DMS of 1.51 nM. The Centre National de Recherches Meteorologiques Earth System Model version 2 (CNRM-ESM2-1) (Séférian et al., 2019) computes DMS concentrations using the biogeochemical Pelagic Interactions Scheme for Carbon and Ecosystem Studies (PISCES) model (Aumont and Bopp, 2006). This includes the processing of DMSP to DMS and phytoplankton functional groups with the destruction of DMS via bacterial decomposition, photolysis, and ventilation. The model computes a weighted
265 annual global mean DMS of 1.98 nM. The Norwegian Earth System Model, version 2 with Low resolution atmosphere-land and Medium resolution ocean sea-ice (NorESM2-LM) (Seland et al., 2020) does not describe the conversion of DMSP to DMS like in PISCES, but instead, it directly computes DMS as a function of temperature resulting in an weighted annual global mean DMS of 1.98 nM.

The Model for Interdisciplinary Research On Climate, Earth System version 2 for Long-term simulations (MIROC-ES2L)
270 (Hajima et al., 2020) computes the seawater DMS concentrations using modified parametrization of Simó and Dachs (Simó and Dachs, 2002) that use MLD and chlorophyll in two regimes (open ocean and shallow mixed water), depending on the chlorophyll to MLD ratio. This results in a weighted annual global mean DMS of 1.77 nM. The United Kingdom Earth System Model, version 1, with Low resolution for both atmosphere-land and ocean-sea ice (UKESM1-0-LL) (Sellar et al., 2019) is used to compute DMS concentration within the biogeochemical Model of Ecosystem Dynamics, nutrient Utilization, Sequestration and Acidification (MEDUSA) (Yool et al., 2013) based on the parametrization given by Anderson (Anderson
275 et al., 2001) in which DMS concentrations depend on a logarithmic function of light, chlorophyll and nutrients. The parameterization used in this model results in a weighted annual global mean DMS of 1.78 nM.

CNRM-ESM2-1 and NorESM2-LM are prognostic models that include marine biota that include sinks and sources of DMS/DMSP, while MIROC-ES2L and UKESM1-0-LL are diagnostic models that use empirical parametrization based on
280 chlorophyll and other parameters (Bock et al., 2021). From Table 1, it can be observed that the global area weighted annual mean DMS range (1.51-1.98 nM) of all these models is close to the weighted annual mean DMS of W20 (1.75 nM) and G18 (1.69 nM). The area weighted global annual means computed by the interpolation-based approach (H22) is significantly higher (2.28 nM) than these models. Most models follow the parametrization approach in order to define the production and destruction process of DMS with environmental/biogeochemical parameters, which depend on our understanding of the
285 underlying processes. If not defined or initiated properly, it can lead to large differences in the estimations. Hence, it should



be noted that although most of these models predict the annual global mean in a similar range, the geographical distribution can show large differences (Hulswar et al., 2022; Belviso et al., 2004b; Bock et al., 2021; Wang et al., 2020b).

4 Conclusions

In this study, we compared the latest interpolation-based and two parameterization-based seawater DMS estimations, which are used for calculating the sea-air fluxes of DMS in conjunction with a sea-air exchange parameterization. The interpolation-based method is easy to implement but results in a relatively higher area the weighted global annual mean DMS (2.28 nM for H22). The parameterization-based methods define a non-linear relationship between DMS and environmental/biogeochemical parameters through regression analysis and estimate lower weighted annual mean DMS compared to the interpolation-based method (1.69 nM for G18 and 1.75 nM for W20). W20 estimates ~3.4 % more weighted global mean DMS when compared with G18, but also shows a lot of geographical heterogeneity. In the case of interpolation-based climatology (H22), the DMS estimate is biased towards regions where observations are frequently taken or towards the region of blooms. The method may give low/high DMS depending on the sampling bias. For example, low DMS values are estimated in April in the northern polar region as compared to March and May (> 60° N) (Fig. 3a). Thus, the interpolation method is not free from regional biases particularly in Arctic region. The parameterization-based approaches depend heavily on the resolution of the proxy parameters. G18 does not show peak values in the Southern Ocean during Austral summer probably due to 1°×1° resolution but there is coastal enhancement at higher resolution and the method explains 50-57 % DMS variability compared to observations, while W20 explains 66 % DMS variability. G18 shows lower values in the Southern Ocean compared to the northern hemisphere. This low DMS in southern ocean is one of the limitations of G18 method. Comparatively, W20 performs better than G18 in the southern hemisphere. However, not all blooms are resolved which could be due to the global filtering of DMS values where DMS > 100 nM before training the ANN model. The filtering of response variable (DMS) and the predictors is probably done as ANN model is sensitive to outlier points that could lead overfitting of model. The annual mean of G18 and W20 is within the range of biogeochemical models (1.51-1.98 nM) but does not necessarily show the same geographical distribution. McNabb and Tortell (2023) trained an ensemble ANN model in Southern Ocean with DMS concentration values more than 100 nM at high resolution (20 km×20 km) which was able to capture DMS hotspots in Southern Ocean. . The results of our analysis suggest that machine learning-based estimations have the potential to predict DMS accurately but need reliable high-resolution input data. It can also capture mesoscale variability, which the interpolation-based methods do not. However, these estimations need a large dataset across different biogeochemical provinces to train the models. Another machine learning known as Gaussian Process Regression (GPR) was recently applied by Mansour et al.(2023) which was able to address ~71 % DMS variability at high temporal and spatial scale in North Atlantic Ocean as compared to observations. With fewer DMS points (~ 2236) the model results show that this can be an efficient tool for obtaining seawater DMS concentration and it may be successful in other oceanic regions or entire global ocean as well. Finally, the inter-annual trends were calculated for the parameterization-based methods and showed a positive trend in both G18 (6.94 ± 1.44 % decade⁻¹) and W20 (3.53 ± 0.53 %



decade⁻¹). This analysis using SeaWiFS data shows that there is increase in DMS concentration over the period from 1998 to 2010. In order to obtain past and future DMS projections, it is not possible to obtained from the satellite-based products as these products are available for limited number of years which could be solved through the predictors obtained from CMIP5 and CMIP6 reconstruct models. It should be noted that there is considerable uncertainty in the estimated DMS concentration and global distributions due to biases in observations, unsuitable global filtering for all regions, incorrect interpolation, and sensitivity of coefficients in parameterization methods. These uncertainties in calculating seawater DMS concentration can lead to uncertainty in DMS fluxes, discussed in a subsequent paper (Joge et al., in prep; referred to as Joge: Part B).

320

325 **Data availability**

All the data used here are publicly available and links are provided in the manuscript.

Competing Interests

The authors declare that they have no conflict of interest.

Author Contributions

330 ASM conceptualized the study. SJ analyzed the data with help from SH. CM, MG, TB and RS helped with the data, ideas and understanding of the study. SJ and ASM wrote the manuscript with the help of all the coauthors.

Acknowledgements

The Indian Institute of Tropical Meteorology is funded by the Ministry of Earth Sciences, Government of India. MG and RS acknowledge support from the European Research Council (ERC) under the European Union's Horizon 2020 research and innovation program (grant agreement #834162, SUMMIT Advanced Grant to RS), and the Spanish Government through grant GOOSE (PID2022_140872NB_I00) as well as the "Severo Ochoa Centre of Excellence" accreditation grant CEX2019-000928-S.

335

References

Anderson, T. R., Spall, S. A., Yool, A., Cipollini, P., Challenor, P. G., and Fasham, M. J. R.: Global fields of sea surface dimethylsulfide predicted from chlorophyll, nutrients and light, *J. Mar. Syst.*, 30, 1–20, [https://doi.org/10.1016/S0924-7963\(01\)00028-8](https://doi.org/10.1016/S0924-7963(01)00028-8), 2001.

340

Andreae, M. O.: Dimethylsulfide in the water column and the sediment porewaters of the Peru upwelling area, *Limnol. Oceanogr.*, 30, 1208–1218, <https://doi.org/10.4319/lo.1985.30.6.1208>, 1985.

Andreae, M. O. and Barnard, W. R.: The marine chemistry of dimethylsulfide, *Mar. Chem.*, 14, 267–279,



- 345 [https://doi.org/10.1016/0304-4203\(84\)90047-1](https://doi.org/10.1016/0304-4203(84)90047-1), 1984.
Andreae, M. O. and Crutzen, P. J.: Atmospheric aerosols: Biogeochemical sources and role in atmospheric chemistry, *Science* (80-.), 276, 1052–1058, 1997.
Astoreca, R., Rousseau, V., and Lancelot, C.: Coloured dissolved organic matter (CDOM) in Southern North Sea waters: Optical characterization and possible origin, *Estuar. Coast. Shelf Sci.*, 85, 633–640, <https://doi.org/10.1016/j.ecss.2009.10.010>,
350 2009.
Aumont, O.: Dimethylsulfoniopropionate (DMSP) and dimethylsulfide (DMS) sea surface distributions simulated from a global three-dimensional ocean carbon cycle model, *J. Geophys. Res.*, 107, <https://doi.org/10.1029/1999jc000111>, 2002.
Aumont, O. and Bopp, L.: Globalizing results from ocean in situ iron fertilization studies, *Global Biogeochem. Cycles*, 20, 1–15, <https://doi.org/10.1029/2005GB002591>, 2006.
- 355 Balch, W. M., Bates, N. R., Lam, P. J., Twining, B. S., Rosengard, S. Z., Bowler, B. C., Drapeau, D. T., Garley, R., Lubelczyk, L. C., Mitchell, C., and Rauschenberg, S.: Factors regulating the Great Calcite Belt in the Southern Ocean and its biogeochemical significance, *Global Biogeochem. Cycles*, 30, 1124–1144, <https://doi.org/10.1002/2016GB005414>, 2016.
Bates, T. S. and Quinn, P. K.: Dimethylsulfide (DMS) in the equatorial Pacific Ocean (1982 to 1996): Evidence of a climate feedback?, *Geophys. Res. Lett.*, 24, 861–864, <https://doi.org/10.1029/97GL00784>, 1997.
- 360 Becagli, S., Lazzara, L., Marchese, C., Dayan, U., Ascanius, S. E., Cacciani, M., Caiazzo, L., Di Biagio, C., Di Iorio, T., di Sarra, A., Eriksen, P., Fani, F., Giardi, F., Meloni, D., Muscari, G., Pace, G., Severi, M., Traversi, R., and Udisti, R.: Relationships linking primary production, sea ice melting, and biogenic aerosol in the Arctic, *Atmos. Environ.*, 136, 1–15, <https://doi.org/10.1016/j.atmosenv.2016.04.002>, 2016.
Bell, T. G., De Bruyn, W., Miller, S. D., Ward, B., Christensen, K., and Saltzman, E. S.: Air-sea dimethylsulfide (DMS) gas transfer in the North Atlantic: Evidence for limited interfacial gas exchange at high wind speed, *Atmos. Chem. Phys.*, 13, 11073–11087, <https://doi.org/10.5194/acp-13-11073-2013>, 2013.
- 365 Belviso, S., Moulin, C., Bopp, L., and Stefels, J.: Assessment of a global climatology of oceanic dimethylsulfide (DMS) concentrations based on SeaWiFS imagery (1998 – 2001), *Can. J. Fish Aquat. Sci.*, 61, 804–816, <https://doi.org/10.1139/F04-001>, 2004a.
- 370 Belviso, S., Bopp, L., Moulin, C., Orr, J. C., Anderson, T. R., Aumont, O., Chu, S., Elliott, S., Maltrud, M. E., and Simó, R.: Comparison of global climatological maps of sea surface dimethyl sulfide, *Global Biogeochem. Cycles*, 18, <https://doi.org/10.1029/2003GB002193>, 2004b.
Bock, J., Michou, M., Nabat, P., Abe, M., Mulcahy, J. P., Olivié, D. J. L., Schwinger, J., Suntharalingam, P., Tjiputra, J., Van Hulten, M., Watanabe, M., Yool, A., and Séférian, R.: Evaluation of ocean dimethylsulfide concentration and emission in
375 CMIP6 models, 18, 3823–3860, <https://doi.org/10.5194/bg-18-3823-2021>, 2021.
Charlson, R. J., Lovelock, J. E., Andreaei, M. O., and Warren, S. G.: Oceanic phytoplankton, atmospheric sulphur, cloud, *Nature*, 330, 1987, 1987.
Chu, S., Elliott, S., and Maltrud, M. E.: Global eddy permitting simulations of surface ocean nitrogen, iron, sulfur cycling,



Chemosphere, 50, 223–235, [https://doi.org/10.1016/S0045-6535\(02\)00162-5](https://doi.org/10.1016/S0045-6535(02)00162-5), 2003.

- 380 Collins, W. J., Bellouin, N., Doutriaux-Boucher, M., Gedney, N., Halloran, P., Hinton, T., Hughes, J., Jones, C. D., Joshi, M., Liddicoat, S., Martin, G., O'Connor, F., Rae, J., Senior, C., Sitch, S., Totterdell, I., Wiltshire, A., and Woodward, S.: Development and evaluation of an Earth-System model - HadGEM2, *Geosci. Model Dev.*, 4, 1051–1075, <https://doi.org/10.5194/gmd-4-1051-2011>, 2011.
- Elliott, S.: Dependence of DMS global sea-air flux distribution on transfer velocity and concentration field type, *J. Geophys. Res.*, 114, G02001, <https://doi.org/10.1029/2008JG000710>, 2009.
- 385 Galí, M. and Simó, R.: A meta-analysis of oceanic DMS and DMSP cycling processes: Disentangling the summer paradox, *Global Biogeochem. Cycles*, 29, 496–515, <https://doi.org/10.1002/2014GB004940>, 2015.
- Galí, M., Devred, E., Levasseur, M., Royer, S. J., and Babin, M.: A remote sensing algorithm for planktonic dimethylsulfoniopropionate (DMSP) and an analysis of global patterns, *Remote Sens. Environ.*, 171, 171–184, <https://doi.org/10.1016/j.rse.2015.10.012>, 2015.
- 390 Galí, M., Levasseur, M., Devred, E., Simó, R., and Babin, M.: Sea-surface dimethylsulfide (DMS) concentration from satellite data at global and regional scales, 15, 3497–3519, <https://doi.org/10.5194/bg-15-3497-2018>, 2018.
- Galí, M., Devred, E., Pérez, G. L., Kieber, D. J., and Simó, R.: Global Ocean dimethylsulfide photolysis rates quantified with a spectrally and vertically resolved model, *Limnol. Oceanogr. Lett.*, 8, 760–769, <https://doi.org/10.1002/lol2.10342>, 2023.
- 395 Geiger, H., Kleffmann, J., and Wiesen, P.: Smog chamber studies on the influence of diesel exhaust on photosmog formation, *Atmos. Environ.*, 36, 1737–1747, [https://doi.org/10.1016/S1352-2310\(02\)00175-9](https://doi.org/10.1016/S1352-2310(02)00175-9), 2002.
- Gourdal, M., Lizotte, M., Massé, G., Gosselin, M., Poulin, M., Scarratt, M., Charette, J., and Levasseur, M.: Dimethyl sulfide dynamics in first-year sea ice melt ponds in the Canadian Arctic Archipelago, 15, 3169–3188, <https://doi.org/10.5194/bg-15-3169-2018>, 2018.
- 400 Hajima, T., Watanabe, M., Yamamoto, A., Tatebe, H., Noguchi, M. A., Abe, M., Ohgaito, R., Ito, A., Yamazaki, D., Okajima, H., Ito, A., Takata, K., Ogochi, K., Watanabe, S., and Kawamiya, M.: Development of the MIROC-ES2L Earth system model and the evaluation of biogeochemical processes and feedbacks, *Geosci. Model Dev.*, 13, 2197–2244, <https://doi.org/10.5194/gmd-13-2197-2020>, 2020.
- Halloran, P. R., Bell, T. G., and Totterdell, I. J.: Can we trust empirical marine DMS parameterisations within projections of future climate?, 7, 1645–1656, <https://doi.org/10.5194/bg-7-1645-2010>, 2010.
- Hawkings, J. R., Skidmore, M. L., Wadham, J. L., Priscu, J. C., Morton, P. L., Hatton, J. E., Gardner, C. B., Kohler, T. J., Stibal, M., Bagshaw, E. A., Steigmeyer, A., Barker, J., Dore, J. E., Berry Lyons, W., Tranter, M., and Spencer, R. G. M.: Enhanced trace element mobilization by Earth's ice sheets, *Proc. Natl. Acad. Sci. U. S. A.*, 117, 31648–31659, <https://doi.org/10.1073/pnas.2014378117>, 2020.
- 410 Hayashida, H., Carnat, G., Galí, M., Monahan, A. H., Mortenson, E., Sou, T., and Steiner, N. S.: Spatiotemporal Variability in Modeled Bottom Ice and Sea Surface Dimethylsulfide Concentrations and Fluxes in the Arctic During 1979–2015, *Global Biogeochem. Cycles*, 34, 1–21, <https://doi.org/10.1029/2019GB006456>, 2020.



- Hulswar, S., Simó, R., Galí, M., Bell, T. G., Lana, A., Inamdar, S., Halloran, P. R., Manville, G., and Mahajan, A. S.: Third revision of the global surface seawater dimethyl sulfide climatology (DMS-Rev3), *Earth Syst. Sci. Data*, 14, 2963–2987, <https://doi.org/10.5194/essd-14-2963-2022>, 2022.
- IPCC: Climate Change 2014: Synthesis Report. Contribution of Working Groups I, II and III to the Fifth Assessment Report of the Intergovernmental Panel on Climate Change, 2014.
- IPCC: Climate Change 2021: The Physical Science Basis. Contribution of Working Group I to the Sixth Assessment Report of the Intergovernmental Panel on Climate Change, 2021.
- Jarníková, T. and Tortell, P. D.: Towards a revised climatology of summertime dimethylsulfide concentrations and sea-air fluxes in the Southern Ocean, *Environ. Chem.*, 13, 364–378, <https://doi.org/10.1071/EN14272>, 2016.
- Kettle, A. J., Andreae, M. O., Amouroux, D., Andreae, T. W., Bates, T. S., Berresheim, H., Bingemer, H., Boniforti, R., Curran, M. A. J., DiTullio, G. R., Helas, G., Jones, G. B., Keller, M. D., Kiene, R. P., Leek, C., Lévassieur, M., Malin, G., Maspero, M., Matrai, P., McTaggart, A. R., Mihelopoulos, N., Nguyen, B. C., Novo, A., Putaud, J. P., Rapsomanikis, S., Roberts, G., Schebeske, G., Sharma, S., Simó, R., Staubes, R., Turner, S., and Uher, G.: A global database of sea surface dimethylsulfide (DMS) measurements and a procedure to predict sea surface DMS as a function of latitude, longitude, and month, *Global Biogeochem. Cycles*, 13, 399–444, <https://doi.org/10.1029/1999GB900004>, 1999.
- Kloster, S., Feichter, J., Maier-Reimer, E., Six, K. D., Stier, P., and Wetzell, P.: DMS cycle in the marine ocean-atmosphere system - A global model study, 3, 29–51, <https://doi.org/10.5194/bg-3-29-2006>, 2006.
- Korhonen, H., Carslaw, K. S., Spracklen, D. V., Mann, G. W., and Woodhouse, M. T.: Influence of oceanic dimethyl sulfide emissions on cloud condensation nuclei concentrations and seasonality over the remote Southern Hemisphere oceans: A global model study, *J. Geophys. Res. Atmos.*, 113, 1–16, <https://doi.org/10.1029/2007JD009718>, 2008.
- Lana, A., Bell, T. G., Simó, R., Vallina, S. M., Ballabrera-Poy, J., Kettle, A. J., Dachs, J., Bopp, L., Saltzman, E. S., Stefels, J., Johnson, J. E., and Liss, P. S.: An updated climatology of surface dimethylsulfide concentrations and emission fluxes in the global ocean, *Global Biogeochem. Cycles*, 25, 1–17, <https://doi.org/10.1029/2010GB003850>, 2011.
- Liss, P. S.: Gas Transfer: Experiments and Geochemical Implications, in: *Air-Sea Exchange of Gases and Particles*, vol. 241, Springer Netherlands, Dordrecht, 241–298, https://doi.org/10.1007/978-94-009-7169-1_5, 1983.
- Longhurst, A., Sathyendranath, S., Platt, T., and Caverhill, C.: An estimate of global primary production in the ocean from satellite radiometer data, *J. Plankton Res.*, 17, 1245–1271, <https://doi.org/10.1093/plankt/17.6.1245>, 1995.
- Mahajan, A. S., De Smedt, I., Biswas, M. S., Ghude, S., Fadnavis, S., Roy, C., and van Roozendaal, M.: Inter-annual variations in satellite observations of nitrogen dioxide and formaldehyde over India, *Atmos. Environ.*, 116, 194–201, <https://doi.org/10.1016/j.atmosenv.2015.06.004>, 2015.
- Mansour, K., Decesari, S., Ceburnis, D., Ovadnevaite, J., and Rinaldi, M.: Machine learning for prediction of daily sea surface dimethylsulfide concentration and emission flux over the North Atlantic Ocean (1998–2021), *Sci. Total Environ.*, 871, 162123, <https://doi.org/10.1016/j.scitotenv.2023.162123>, 2023.
- Manville, G., Bell, T. G., Mulcahy, J. P., Simó, R., Galí, M., Mahajan, A. S., Hulswar, S., and Halloran, P. R.: Global analysis

of the controls on seawater dimethylsulfide spatial variability, 20, 1813–1828, <https://doi.org/10.5194/bg-20-1813-2023>, 2023.

McNabb, B. J. and Tortell, P. D.: Oceanographic controls on Southern Ocean dimethyl sulfide distributions revealed by machine learning algorithms, *Limnol. Oceanogr.*, 1–15, <https://doi.org/10.1002/lno.12298>, 2023.

450 Park, K., Kim, I., Choi, J. O., Lee, Y., Jung, J., Ha, S. Y., Kim, J. H., and Zhang, M.: Unexpectedly high dimethyl sulfide concentration in high-latitude Arctic sea ice melt ponds, *Environ. Sci. Process. Impacts*, 21, 1642–1649, <https://doi.org/10.1039/c9em00195f>, 2019.

Park, K. T., Lee, K., Kim, T. W., Yoon, Y. J., Jang, E. H., Jang, S., Lee, B. Y., and Hermansen, O.: Atmospheric DMS in the Arctic Ocean and Its Relation to Phytoplankton Biomass, *Global Biogeochem. Cycles*, 32, 351–359, 455 <https://doi.org/10.1002/2017GB005805>, 2018.

Reygondeau, G., Longhurst, A., Martinez, E., Beaugrand, G., Antoine, D., and Maury, O.: Dynamic biogeochemical provinces in the global ocean, *Global Biogeochem. Cycles*, 27, 1046–1058, <https://doi.org/10.1002/gbc.20089>, 2013.

Riseman, S. F. and DiTullio, G. R.: Particulate dimethylsulfoniopropionate and dimethylsulfoxide in relation to iron availability and algal community structure in the Peru Upwelling System, *Can. J. Fish. Aquat. Sci.*, 61, 721–735, 460 <https://doi.org/10.1139/F04-052>, 2004.

Royer, S.-J., Mahajan, A. S., Galí, M., Saltzman, E., and Simó, R.: Small-scale variability patterns of DMS and phytoplankton in surface waters of the tropical and subtropical Atlantic, Indian, and Pacific Oceans, *Geophys. Res. Lett.*, 42, 475–483, <https://doi.org/10.1002/2014GL062543>, 2015.

Saint-Macary, A. D., Marriner, A., Deppeler, S., Safi, K. A., and Law, C. S.: Dimethyl sulfide cycling in the sea surface microlayer in the southwestern Pacific – Part 2: Processes and rates, *Ocean Sci.*, 18, 1559–1571, <https://doi.org/10.5194/os-18-1559-2022>, 2022.

Séférian, R., Nabat, P., Michou, M., Saint-Martin, D., Voltaire, A., Colin, J., Decharme, B., Delire, C., Berthet, S., Chevallier, M., Sénési, S., Franchisteguy, L., Vial, J., Mallet, M., Joetzjer, E., Geoffroy, O., Guérémy, J. F., Moine, M. P., Msadek, R., Ribes, A., Rocher, M., Roehrig, R., Salas-y-Méllia, D., Sanchez, E., Terray, L., Valcke, S., Waldman, R., Aumont, O., Bopp, 470 L., Deshayes, J., Éthé, C., and Madec, G.: Evaluation of CNRM Earth System Model, CNRM-ESM2-1: Role of Earth System Processes in Present-Day and Future Climate, *J. Adv. Model. Earth Syst.*, 11, 4182–4227, <https://doi.org/10.1029/2019MS001791>, 2019.

Seland, Ø., Bentsen, M., Olivie, D., Toniazzo, T., Gjermundsen, A., Graff, L. S., Debernard, J. B., Gupta, A. K., He, Y. C., Kirkevåg, A., Schwinger, J., Tjiputra, J., Schanke Aas, K., Bethke, I., Fan, Y., Griesfeller, J., Grini, A., Guo, C., Ilicak, M., 475 Karset, I. H. H., Landgren, O., Liakka, J., Moseid, K. O., Nummelin, A., Spensberger, C., Tang, H., Zhang, Z., Heinze, C., Iversen, T., and Schulz, M.: Overview of the Norwegian Earth System Model (NorESM2) and key climate response of CMIP6 DECK, historical, and scenario simulations, 6165–6200 pp., <https://doi.org/10.5194/gmd-13-6165-2020>, 2020.

Sellar, A. A., Jones, C. G., Mulcahy, J. P., Tang, Y., Yool, A., Wiltshire, A., O’Connor, F. M., Stringer, M., Hill, R., Palmieri, J., Woodward, S., de Mora, L., Kuhlbrodt, T., Rumbold, S. T., Kelley, D. I., Ellis, R., Johnson, C. E., Walton, J., Abraham, N. 480 L., Andrews, M. B., Andrews, T., Archibald, A. T., Berthou, S., Burke, E., Blockley, E., Carslaw, K., Dalvi, M., Edwards, J.,



Folberth, G. A., Gedney, N., Griffiths, P. T., Harper, A. B., Hendry, M. A., Hewitt, A. J., Johnson, B., Jones, A., Jones, C. D., Keeble, J., Liddicoat, S., Morgenstern, O., Parker, R. J., Predoi, V., Robertson, E., Siahahan, A., Smith, R. S., Swaminathan, R., Woodhouse, M. T., Zeng, G., and Zerroukat, M.: UKESM1: Description and Evaluation of the U.K. Earth System Model, *J. Adv. Model. Earth Syst.*, 11, 4513–4558, <https://doi.org/10.1029/2019MS001739>, 2019.

485 Shenoy, D. M. and Kumar, M. D.: Variability in abundance and fluxes of dimethyl sulphide in the Indian Ocean, *Biogeochemistry*, 83, 277–292, <https://doi.org/10.1007/s10533-007-9092-4>, 2007.

Shenoy, D. M., Joseph, S., Kumar, M. D., and George, M. D.: Control and interannual variability of dimethyl sulfide in the Indian ocean, *J. Geophys. Res. Atmos.*, 107, 1–9, <https://doi.org/10.1029/2001JD000371>, 2002.

490 Simó, R.: Production of atmospheric sulfur by oceanic plankton : biogeochemical , ecological and evolutionary links, *Trends Ecol. Evol.*, 16, 287–294, 2001.

Simó, R. and Dachs, J.: Global ocean emission of dimethylsulfide predicted from biogeophysical data, *Global Biogeochem. Cycles*, 16, <https://doi.org/10.1029/2001GB001829>, 2002.

Six, K. D. and Maier-Reimer, E.: What controls the oceanic dimethylsulfide (DMS) cycle? A modeling approach, *Global Biogeochem. Cycles*, 20, 1–12, <https://doi.org/10.1029/2005GB002674>, 2006.

495 Sørensen, H. L., Thamdrup, B., Jeppesen, E., Rysgaard, S., and Glud, R. N.: Nutrient availability limits biological production in Arctic sea ice melt ponds, *Polar Biol.*, 40, 1593–1606, <https://doi.org/10.1007/s00300-017-2082-7>, 2017.

Stefels, J., Steinke, M., Turner, S., Malin, G., and Belviso, S.: Review: Environmental constraints on the production and removal of the climatically active gas dimethylsulphide (DMS) and implications for ecosystem modelling., *Biogeochemistry*, 83, 245–275, <https://doi.org/10.1007/s10533-007-9091-5>, 2007.

500 TAPIAS,M.G.:DMS-SAT_GLOBAL_MONTHLY_DMS_DMSPt_CLIM_v1.0.0,
<https://doi.org/10.5281/zenodo.2558511>, February 2019.

Toole, D. A., Kieber, D. J., Kiene, R. P., Siegel, D. A., and Nelson, N. B.: Photolysis and the dimethylsulfide (DMS) summer paradox in the Sargasso Sea, *Limnol. Oceanogr.*, 48, 1088–1100, <https://doi.org/10.4319/lo.2003.48.3.1088>, 2003.

505 Vallina, S. M. and Simó, R.: Strong relationship between DMS and the solar radiation dose over the global surface ocean, *Science (80-.)*, 315, 506–508, <https://doi.org/10.1126/science.1133680>, 2007.

Vogt, M., Vallina, S. M., Buitenhuis, E. T., Bopp, L., and Le Quéré, C.: Simulating dimethylsulphide seasonality with the Dynamic Green Ocean Model PlankTOM5, *J. Geophys. Res. Ocean.*, 115, 1–21, <https://doi.org/10.1029/2009JC005529>, 2010.

510 Wang, S., Maltrud, M. E., Burrows, S. M., Elliott, S. M., and Cameron-Smith, P.: Impacts of Shifts in Phytoplankton Community on Clouds and Climate via the Sulfur Cycle, *Global Biogeochem. Cycles*, 32, 1005–1026, <https://doi.org/10.1029/2017GB005862>, 2018a.

Wang, S., Maltrud, M., Elliott, S., Cameron-Smith, P., and Jonko, A.: Influence of dimethyl sulfide on the carbon cycle and biological production, *Biogeochemistry*, 138, 49–68, <https://doi.org/10.1007/s10533-018-0430-5>, 2018b.

Wang, W.-L., Song, G., Primeau, F., Saltzman, E., Bell, T., and Moore, J. K.: Global ocean dimethyl sulfide climatology estimated from observations and an artificial neural network, <https://doi.org/10.5281/zenodo.3833233>, May 2020a.



- 515 Wang, W. L., Song, G., Primeau, F., Saltzman, E. S., Bell, T. G., and Moore, K. K.: Global ocean dimethyl sulfide climatology estimated from observations and an artificial neural network, *17*, 5335–5354, <https://doi.org/10.5194/bg-17-5335-2020>, 2020b.
- Weatherhead, E. C., Reinsel, G. C., Tiao, G. C., Meng, X. L., Choi, D., Cheang, W. K., Keller, T., DeLuisi, J., Wuebbles, D. J., Kerr, J. B., Miller, A. J., Oltmans, S. J., and Frederick, J. E.: Factors affecting the detection of trends: Statistical considerations and applications to environmental data, *J. Geophys. Res. Atmos.*, *103*, 17149–17161, <https://doi.org/10.1029/98JD00995>, 1998.
- 520 Yool, A., Popova, E. E., and Anderson, T. R.: MEDUSA-2.0: An intermediate complexity biogeochemical model of the marine carbon cycle for climate change and ocean acidification studies, *Geosci. Model Dev.*, *6*, 1767–1811, <https://doi.org/10.5194/gmd-6-1767-2013>, 2013.
- Zhang, M., Marandino, C. A., Yan, J., Wu, Y., Park, K., Sun, H., Gao, Z., and Xu, S.: Unravelling Surface Seawater DMS Concentration and Sea-To-Air Flux Changes After Sea Ice Retreat in the Western Arctic Ocean, *Global Biogeochem. Cycles*, *35*, 1–15, <https://doi.org/10.1029/2020GB006796>, 2021.
- 525 Zindler, C., Peeken, I., Marandino, C. A., and Bange, H. W.: Environmental control on the variability of DMS and DMSP in the Mauritanian upwelling region, *9*, 1041–1051, <https://doi.org/10.5194/bg-9-1041-2012>, 2012.

530 **Table:**

Table 1. Summary of different methods and respective annual mean DMS.

Climatology/Model	Area Weighted Global DMS Mean (nM)	Characteristics of DMS Scheme	Reference
H22	2.28	Interpolation	(Hulswar et al., 2022)
W20	1.75	Machine Learning-based Parametrization	(Wang et al., 2020)
G18	1.69	Simple Regression-based Parametrization	(Galí et al., 2018)
Au02	1.70	Process Model Parametrization	(Aumont, 2002)
Chu03	1.51	Prognostic Model	(Chu et al., 2003)
CNRM-ESM2-1	1.98	Prognostic Model	(Séférian et al., 2019)
NorESM2-LM	1.98	Prognostic Model	(Seland et al., 2020)
MIROC-ES2L	1.77	Diagnostic Model	(Hajima et al., 2020)
UKESM1-0-LL	1.78	Diagnostic Model	(Sellar et al., 2019)



535 **Figures:**

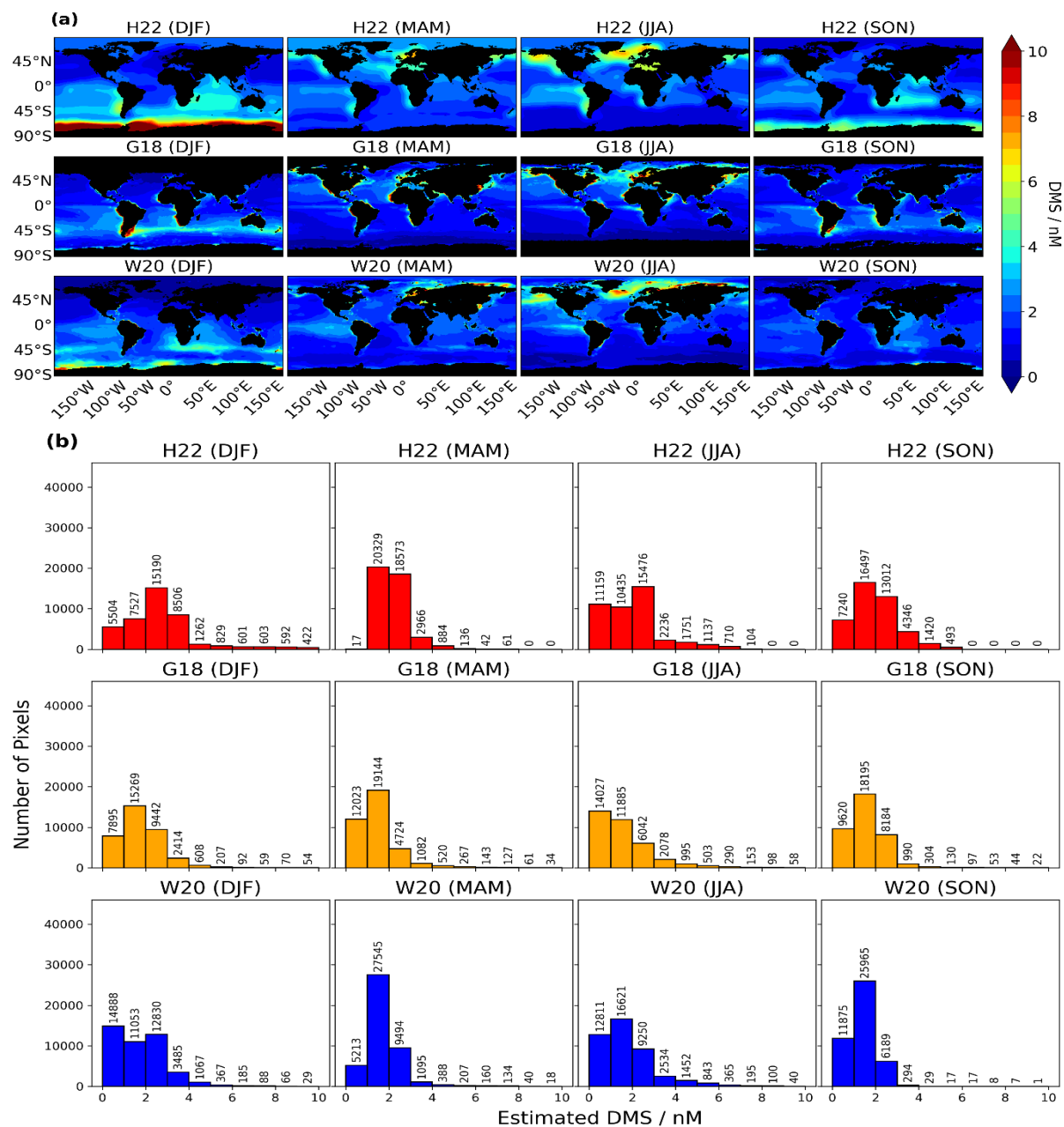


Figure 1: (a) Global seasonal climatologies of H22, G18, and W20 for austral summer (DJF), spring (MAM), boreal summer (JJA), and autumn (SON) seasons. For all the climatologies, most of the pixels show DMS concentration less than 3 nM in oligotrophic regions and higher concentration along coastal regions. (b) G18 and W20 captured DMS values more than 8 nM while H22 did not (except DJF season). H22 predicts highest number of pixels in the 3-4 nM range and more than 2000 pixels showing concentrations above 6 nM in DJF season.

540

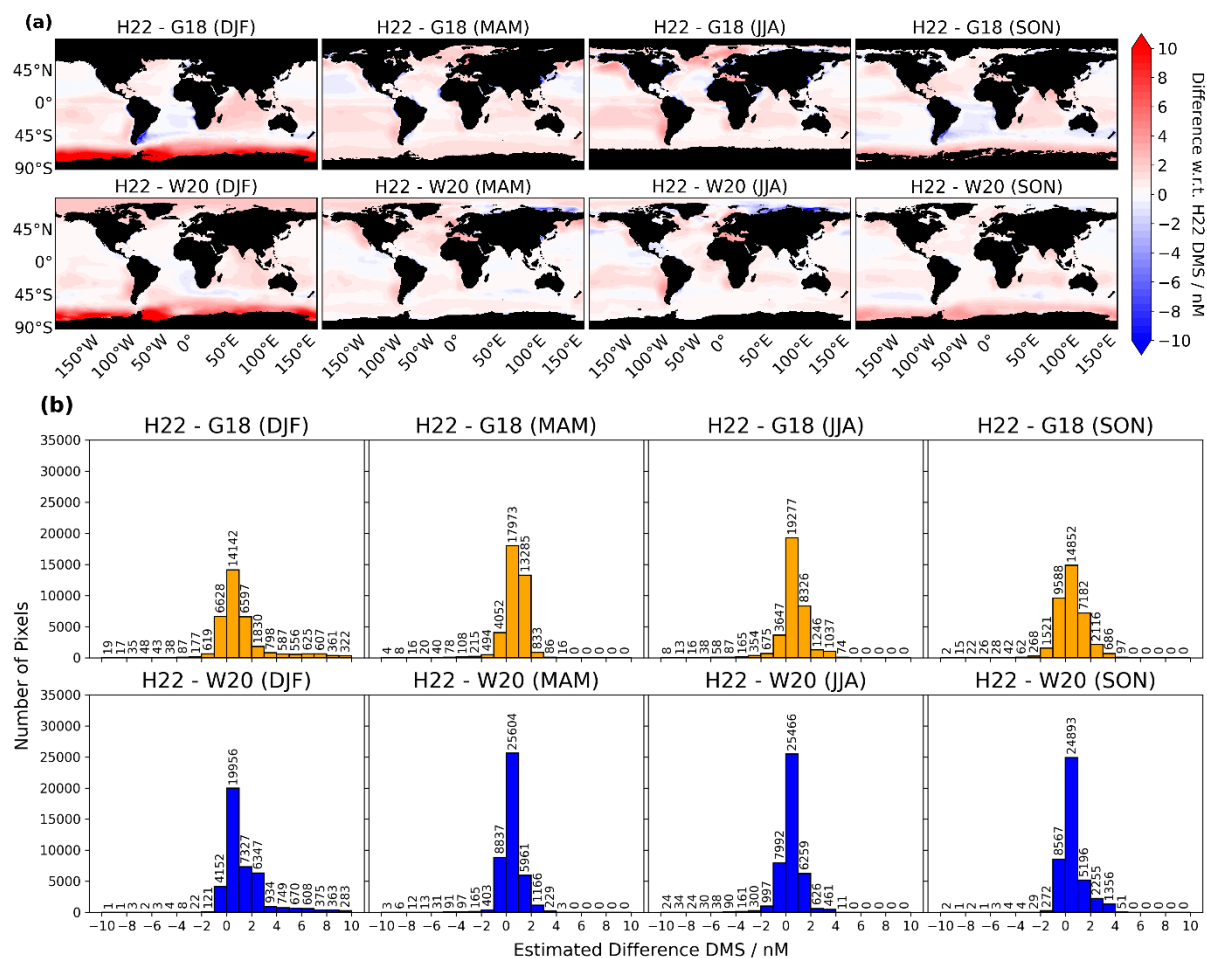


Figure 2: (a) Differences between the H22 climatology compared with G18, W20. From all the seasons, the maximum difference between H22 and G18 is -14.74 nM during DJF in the Argentinian basin and -29.03 nM for W20 during MAM in the North Sea. (b) A histogram represents the total number of pixels for each difference bin. The differences between H22 and G18 or W20 are not exactly centered around zero, with most pixels showing higher values in the H22 estimation.

545

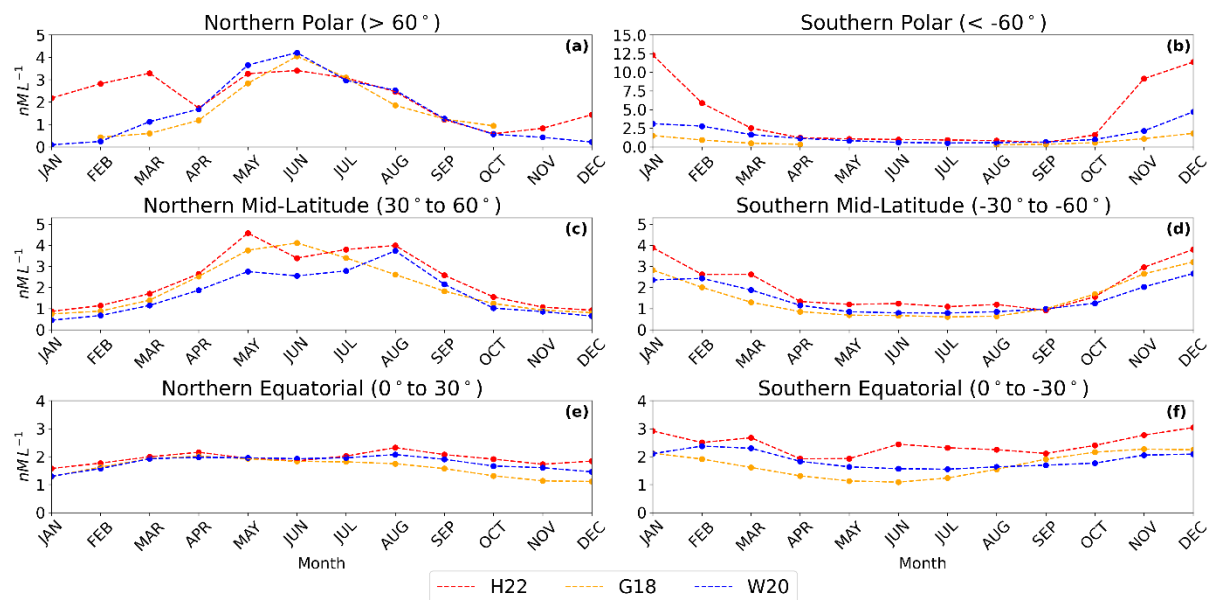


Figure 3: Latitudinal means for each month for all climatologies used in this study. Large differences are observed in the southern polar region between the interpolation-based and parameterization-based climatologies. G18 has the lowest values of the three in Southern Polar region while the estimates are close to W20 in northern equatorial band.

550

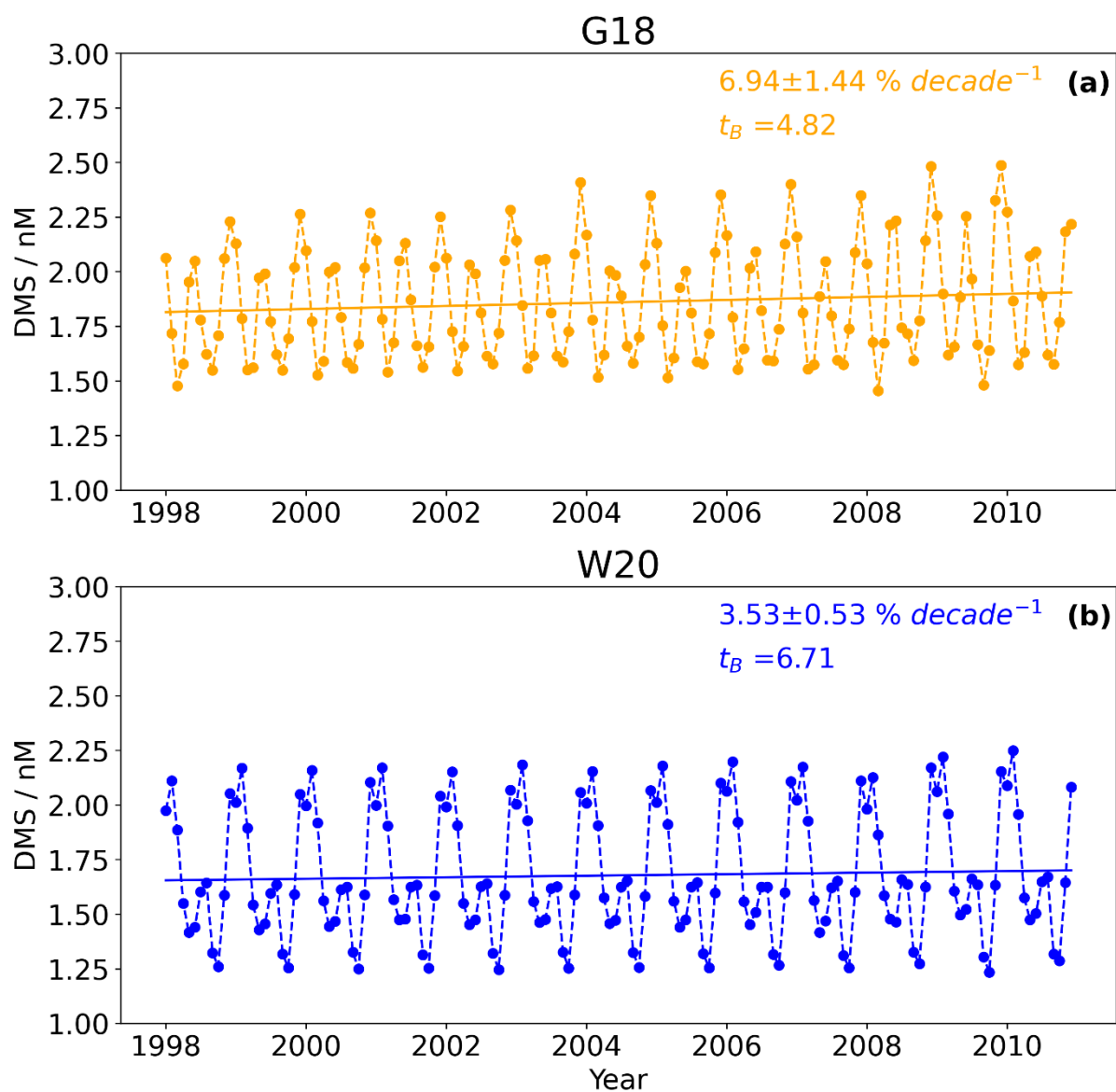


Figure 4: Inter-annual trends in all the seawater DMS concentrations for (a) G18 and (b) W20. The inter-annual trend is significant and positive. The trend is calculated using the bootstrap resampling method.

555